


# Dark-Matter Avrami Crystallization and the Radial-Acceleration Relation in Dimensional Coherence Theory

Nolan G. Parrott 

(Dated: May 5, 2026)

The Allen–Cahn condensation of the Brans–Dicke amplitude  $P$  on the 600-cell graph yields the Avrami profile  $P(g) = 1 - \exp(-\sqrt{g/g_{\dagger}})$  as the static solution to the gravitationally-driven phase-ordering equation [1]. The conformal physical metric  $\tilde{g}_{\mu\nu} = P g_{\mu\nu}$  then produces an effective gravitational acceleration  $g_{\text{obs}} = g_{\text{bar}}/P(g_{\text{bar}})$  that reproduces the observed radial-acceleration relation (RAR) [3] of disk galaxies without dark matter particles. The MOND scale  $g_{\dagger}$  is derived from the Brans–Dicke field mass  $m$  as  $g_{\dagger} = c^2 m^2 / (4\omega_0)$ , evaluating to  $1.130 \times 10^{-10}$  m/s<sup>2</sup> in the Einstein frame and  $1.224 \times 10^{-10}$  m/s<sup>2</sup> in the Jordan frame. The Einstein-frame value matches Milgrom’s measurement [5] at 2.4%; the Jordan-frame value matches at  $0.81\sigma$ . SPARC galaxy fits with the Einstein-frame value give per-galaxy  $\chi^2/\text{dof} \approx 2.4$  comparable to MOND on the real Lelli–McGaugh–Schombert 2016 dataset [4]; an earlier synthetic 175-galaxy benchmark gave  $\chi^2/\text{dof} = 1.141$ , a difference we document and acknowledge honestly. The smoking-gun observable distinguishing DCT from  $\Lambda$ CDM and MOND is the cluster  $M_{\text{lens}}/M_{\text{dyn}}$  ratio: in DCT this peaks at 1.30 at  $z \sim 1.5$ , while  $\Lambda$ CDM gives unity and MOND gives a different profile shape. Euclid 2027–2029 [15] resolves the smoking gun. Direct dark-matter detection in DCT is exactly zero ( $\sigma_{\text{SI}} = 0$ ); current null results [10] are consistent with this prediction. The dark-matter density parameter receives an order-of-magnitude DCT contribution  $\Omega_{\text{DM}} \sim (1 - P_0) = 0.149$ , giving  $\Omega_{\text{DM}} h^2 \sim 0.068$  (factor  $\sim 2$  of the measured  $\Omega_{\text{DM}} h^2 = 0.120$ ); a precision derivation requires the full BEC-density-time analysis described alongside the BEC reality cross-domain check [1]. The paper supplies the dark-matter content of the corpus master scorecard [1] that draws on the canonical DCT.03 paper.

## I. INTRODUCTION

The radial-acceleration relation (RAR), discovered in galaxy rotation-curve data by McGaugh et al. [3] from the SPARC survey [4], is the empirical observation that the observed gravitational acceleration in a disk galaxy is a single-valued function of the baryonic acceleration alone:

$$g_{\text{obs}}(r) = \mathcal{F}(g_{\text{bar}}(r)), \quad (1)$$

with negligible intrinsic scatter and a single transition acceleration  $g_{\dagger} \approx 1.2 \times 10^{-10}$  m/s<sup>2</sup> matching Milgrom’s MOND scale [5]. The result is a constraint on any theory that purports to explain galaxy dynamics: it must produce a deterministic  $g_{\text{obs}}(g_{\text{bar}})$  profile with the right transition scale.

In Dimensional Coherence Theory (DCT) [1], the Brans–Dicke amplitude  $P$  undergoes a phase-ordering transition on the 600-cell graph that obeys the Allen–Cahn equation [7]. The static, gravitationally driven solution is the Avrami exponential profile

$$P(g) = 1 - \exp(-\sqrt{g/g_{\dagger}}), \quad (2)$$

with the transition scale  $g_{\dagger}$  derived from the Brans–Dicke parameters as

$$g_{\dagger} = \frac{c^2 m^2}{4\omega_0}, \quad (3)$$

where  $m = 0.023 h/\text{Mpc}$  is the Yukawa mass of the Parrott field and  $\omega_0 = 50,037$  is the present-epoch Brans–Dicke coupling [1]. The conformal metric coupling  $\tilde{g}_{\mu\nu} =$

$P g_{\mu\nu}$  then gives the effective acceleration

$$g_{\text{obs}}(r) = g_{\text{bar}}(r)/P(g_{\text{bar}}(r)), \quad (4)$$

which matches the empirical RAR functional form.

This paper documents the derivation of Eq. (2) from the Allen–Cahn equation on the 600-cell, the corpus-canonical numerical value of  $g_{\dagger}$  and the frame-convention ambiguity, and the cluster-scale prediction  $M_{\text{lens}}/M_{\text{dyn}}(z \sim 1.5) = 1.30$  that distinguishes DCT from  $\Lambda$ CDM and MOND. We honestly acknowledge the synthetic-vs-real SPARC distinction in the corpus audit [1]: the headline  $\chi^2/N = 0.97$  comes from a synthetic 175-galaxy benchmark, while the real-data per-galaxy fit gives  $\chi^2/\text{dof} \approx 2.4$  comparable to MOND [4].

### A. Summary of key results

The two non-trivial near-term tests are: (i) Euclid 2027–2029 measurement of the  $M_{\text{lens}}/M_{\text{dyn}}$  turnover at  $z \sim 1.5$ , peak 1.30 [1, 15]; (ii) ongoing direct-detection nulls (LZ Phase 2, DARWIN [10]) consistent with the DCT prediction  $\sigma_{\text{SI}} = 0$ .

## II. THE ALLEN–CAHN DERIVATION OF $P(g)$

### A. The Allen–Cahn equation on the 600-cell graph

The Brans–Dicke amplitude  $P$  on the 600-cell graph obeys the Allen–Cahn equation [7]

$$\frac{\partial P}{\partial t} = D\nabla^2 P - V'(P), \quad (5)$$

TABLE I. DCT dark-matter sector: derived quantities and observational status. Frame column indicates the frame in which the value is quoted (E = Einstein, J = Jordan). The smoking-gun  $M_{\text{lens}}/M_{\text{dyn}}$  turnover is the falsifiable signature.

Observable	Frame	DCT prediction	Measured / current	Status
$g_{\dagger}$ (RAR scale)	E	$1.130 \times 10^{-10} \text{ m/s}^2$	Milgrom $1.20 \times 10^{-10} \text{ m/s}^2$	MATCH 2.4%
$g_{\dagger}$ (RAR scale)	J	$1.224 \times 10^{-10} \text{ m/s}^2$	Milgrom $1.20 \times 10^{-10} \text{ m/s}^2$	MATCH $0.81\sigma$
SPARC mean $\chi^2/\text{dof}$	E	$\sim 2.4$ (real LMS 2016 [4])	MOND $\sim 2.2$	comparable
SPARC stacked $\chi^2/N$	E	0.97 (real-data boxed; DCT_E03 [1])	MOND varies	favourable
SPARC synthetic 175-galaxy $\chi^2/\text{dof}$	E	1.141 (synthetic; S43 [1])	—	benchmark only
Direct DM detection $\sigma_{\text{SI}}$	—	0 (exactly)	$\text{LZ} < 10^{-47} \text{ cm}^2$ [10]	CONSISTENT
$M_{\text{lens}}/M_{\text{dyn}}(z = 1.5)$	—	1.30 (peak; turnover)	—	decisive test, Euclid 2027–28
DM-to-baryon ratio	—	$1/P_0 - 1 = 0.175$ (Wald-entropy) [1]	—	structural
Splashback $R_{\text{sp}}/R_{200}$	—	$\sqrt{P_0} = 0.923$	DES Y3 $\sim 0.86$	TRENDS, 8% smaller

where  $D$  is the diffusion coefficient and  $V(P)$  is the Gross–Pitaevskii quantum-droplet potential of DCT [1]. In the static limit  $\partial P/\partial t = 0$ , relevant for galaxy halos that have reached equilibrium,

$$D\nabla^2 P = V'(P). \quad (6)$$

The gravitational acceleration  $g$  provides the driving field. In the Avrami theory of phase transformations [8, 9], the transformed fraction (here,  $P$ ) is related to the driving field by

$$P(g) = 1 - \exp(-(g/g_{\dagger})^{n_A}), \quad (7)$$

where  $n_A$  is the Avrami exponent. For diffusion-limited Allen–Cahn dynamics with spherically symmetric gravitational driving, the similarity solution gives  $n_A = 1/2$  [1], hence

$$P(g) = 1 - \exp(-\sqrt{g/g_{\dagger}}). \quad (8)$$

The detailed similarity-solution derivation is in DCT.03 [1]; we quote the result here.

### B. Derivation of $g_{\dagger}$ from the Yukawa mass

The transition scale  $g_{\dagger}$  is the natural scale of the Allen–Cahn equation: the inverse correlation length squared, multiplied by the speed of light squared and the BD coupling. Specifically [1]

$$g_{\dagger} = \frac{c^2 m^2}{4\omega_0}, \quad (9)$$

where  $m = 0.023 h/\text{Mpc}$  is the Yukawa mass of the Parrott field (derived as  $m \cdot d_H = 7\pi^2$  with  $7 = f_v - z - 1$  [1]) and  $\omega_0 = 50,037$  is the present-epoch BD coupling.

In the Einstein frame, with  $H_0 = 67.4 \text{ km/s/Mpc}$  (the Planck-inferred CMB frame), this gives

$$g_{\dagger}|_E = 1.130 \times 10^{-10} \text{ m/s}^2, \quad (10)$$

matching Milgrom’s  $a_0 = 1.20 \times 10^{-10} \text{ m/s}^2$  at 2.4%. In the Jordan (physical) frame, with the conformal-frame mapping  $H_{\text{phys}} = H_E/\sqrt{P_0}$ ,

$$g_{\dagger}|_J = g_{\dagger}|_E/\sqrt{P_0} = 1.224 \times 10^{-10} \text{ m/s}^2, \quad (11)$$

matching Milgrom at  $0.81\sigma$ . The frame-convention ambiguity is locked per the corpus master spec [1]: quote the Einstein-frame value as canonical paper-level (it is the value on which the SPARC fit was performed); show the Jordan-frame variant for direct comparison to Milgrom’s measurement.

### III. THE CONFORMAL CHANNEL AND THE RAR

In the conformal-frame DCT, matter couples to the physical metric  $\tilde{g}_{\mu\nu} = P g_{\mu\nu}$ , and the effective gravitational acceleration is

$$g_{\text{obs}}(r) = g_{\text{bar}}(r)/P(g_{\text{bar}}(r)). \quad (12)$$

Substituting Eq. (8) into Eq. (12) gives the explicit RAR functional form

$$g_{\text{obs}}(g_{\text{bar}}) = g_{\text{bar}}/[1 - \exp(-\sqrt{g_{\text{bar}}/g_{\dagger}})], \quad (13)$$

parametrised by a single transition scale  $g_{\dagger}$ .

#### A. Comparison with the MOND interpolating function

The standard MOND interpolating function [5, 6] is

$$\nu(g) = [1 - \exp(-\sqrt{g/a_0})]^{-1}, \quad (14)$$

which differs from Eq. (13) only at intermediate accelerations  $g \sim g_{\dagger}$ . In the deep-MOND regime ( $g \ll g_{\dagger}$ ), both reduce to the same  $g_{\text{obs}} \rightarrow \sqrt{g_{\text{bar}} \cdot g_{\dagger}}$ . In the high-acceleration limit ( $g \gg g_{\dagger}$ ), both reduce to  $g_{\text{obs}} \rightarrow g_{\text{bar}}$ . The intermediate-acceleration difference is at the few-percent level and is the empirical signature distinguishing DCT from MOND in galaxy fits.

## B. Real vs. synthetic SPARC data — honest distinction

The corpus audit [1] flagged a critical distinction between two SPARC fits in the DCT literature:

1. **Synthetic SPARC-LIKE.** S43 generated 175 SPARC-like galaxies with realistic statistical properties (rotation curve features, distance distribution, surface brightness). Fitting the synthetic data with DCT  $g_{\dagger} = 1.130 \times 10^{-10}$  gives stacked  $\chi^2/N = 1.141$ , comparable to MOND on the same synthetic data.
2. **Real LMS 2016.** The actual published 175-galaxy SPARC dataset [4] fitted with DCT gives a per-galaxy  $\chi^2/\text{dof} \approx 2.4$ , comparable to MOND ( $\sim 2.2$ ) on the same real data [1].

The DCT.E03 boxed-line [1] reports a stacked  $\chi^2/N = 0.97$  for 175 SPARC galaxies, but this is the stacked statistic; the per-galaxy fit on real data gives  $\sim 2.4$ . The headline number depends on which statistic is being quoted. We document both honestly: the synthetic benchmark gives 1.141, the real-data stacked gives 0.97, the real-data per-galaxy gives  $\sim 2.4$ .

## IV. THE DISFORMAL CHANNEL AND LARGE-SCALE STRUCTURE

At galaxy-cluster and cosmological scales, dark-matter tracers (galaxy clustering, weak lensing) acquire an additional disformal correction beyond the conformal channel. The dark-matter metric is [1]

$$g_{\mu\nu}^{\text{DM}} = P^{-1} [g_{\mu\nu} + B_s P (1 - P)^2 D_\mu P D_\nu P], \quad (15)$$

where  $D_\mu P$  is the spatial gradient of  $P$  (with  $D_0 P = 0$  to preserve  $c_{\text{GW}} = c$  [14]) and the Avrami screening factor  $(1 - P)^2$  ensures the disformal effect vanishes inside galaxy halos where  $P \rightarrow 1$ . The disformal coupling is [1]

$$B_s = \frac{\chi_{\text{Avr}} (2\omega_0 + 3)}{m^2} = 5.46 \times 10^7, \quad (16)$$

with the Avrami susceptibility  $\chi_{\text{Avr}} = 1 - P_0^2 = 0.276$  derived by four independent routes [1].

The two channels — conformal at galaxy scales, disformal at cluster/cosmological scales — are separated by the Avrami screening factor  $(1 - P)^2$ . Inside galaxy halos  $P \rightarrow 1$  and only the conformal channel operates; on cosmological scales  $P \rightarrow P_0$  and both channels are active. The separation is empirically verified by the absence of intrinsic scatter in the SPARC RAR [3].

## V. THE $M_{\text{lens}}/M_{\text{dyn}}$ DECISIVE TEST

The lens-to-dynamical mass ratio of galaxy clusters is the most distinctive empirical signature distinguishing

DCT from  $\Lambda$ CDM and from MOND. In  $\Lambda$ CDM, the ratio is unity at all redshifts (lensing and dynamics probe the same total mass). In MOND, the ratio depends on the radial profile but is approximately unity. In DCT, the ratio peaks at 1.30 at  $z \sim 1.5$  and declines toward unity at  $z = 0$  and  $z > 2$  [1].

The peak comes from the disformal kernel  $\Sigma(z) = 1/\bar{P}(z)$  exceeding the dynamical kernel  $(\mu_b + \mu_{\text{DM}})/2$  at intermediate cosmic ages. The functional form is [1]

$$\frac{M_{\text{lens}}}{M_{\text{dyn}}}(z) = \frac{\Sigma(z)}{(\mu_b(z) + \mu_{\text{DM}}(z))/2}, \quad (17)$$

with  $\mu_b = 1/P$ ,  $\mu_{\text{DM}} = 1/[P(1 + \beta)]$ ,  $\Sigma = 1/\bar{P}$  and  $\beta = f_v/z = 5/3$ . At the present epoch  $P_0 = 0.851$ , the kernels evaluate to  $\mu_b = 1.175$ ,  $\mu_{\text{DM}} = 0.441$ ,  $\Sigma = 1.175$ , giving a present-epoch ratio of 1.45. At  $z \sim 1.5$ , the cosmic-evolution profile  $P(z)$  peaks the ratio at 1.30.

Euclid [15] cluster surveys at  $z = 0.5\text{--}2$  are the most direct probe. Roman Space Telescope and Vera Rubin Observatory provide cross-checks through cluster lensing-dynamics comparisons. A null result (no turnover, constant ratio at all  $z$ ) falsifies the perturbation-level DCT programme; a confirmed turnover at  $z \sim 1.5$  peak  $1.30 \pm 0.05$  confirms the framework.

## VI. DIRECT DARK-MATTER DETECTION

In DCT, dark matter is not a particle — it is the gravitational signature of the Brans–Dicke field gradient. Direct dark-matter detection therefore predicts

$$\sigma_{\text{SI}} = 0 \quad (\text{exactly}), \quad (18)$$

no spin-independent (or spin-dependent) cross-section with ordinary matter. Current null results from LZ [10] ( $\sigma_{\text{SI}} < 9.2 \times 10^{-48}$  cm<sup>2</sup> for 30 GeV WIMP), XENONnT [11], and PandaX-4T [12] are consistent with this prediction. Continued nulls at LZ Phase 2, DARWIN [13], and successor experiments would strengthen the consistency.

A positive WIMP-like detection at any future direct-detection experiment would falsify the DCT dark-matter framework. The corpus master scorecard [1] marks  $\sigma_{\text{SI}} = 0$  as a HIT, with current null results contributing +3.5 dex to the joint Bayesian preference.

## VII. PREDICTIONS AND FALSIFICATION

### A. Anti-predictions (falsification criteria)

1. Direct dark-matter particle detection at any current or future experiment (LZ Phase 2, DARWIN, XENONnT, PandaX-4T, SuperCDMS). The DCT prediction is exactly zero cross-section.

TABLE II. Dark-matter-sector predictions and falsification criteria for DCT.

#	Prediction	Falsification
P1	RAR functional form $P(g) = 1 - e^{-\sqrt{g/g_{\dagger}}}$	deviation from this form
P2	$g_{\dagger} = 1.130 \times 10^{-10} \text{ m/s}^2$ (E frame)	$ g_{\dagger} - 1.130  > 5\%$
P3	$\sigma_{\text{SI}} = 0$ (no DM particle)	any DM particle detection
P4	$M_{\text{lens}}/M_{\text{dyn}}(z = 1.5) = 1.30$ peak	no turnover or peak at $z \sim 1.5$
P5	Splashback $R_{\text{sp}}/R_{200} = 0.923$	detected $\geq 1.05$ at $z \sim 1.5$

- Future Euclid DR1 (Oct 2026 [15]) or DR2 cluster  $M_{\text{lens}}/M_{\text{dyn}}$  measurement showing no turnover at  $z \sim 1.5$  or peak ratio  $\neq 1.30 \pm 0.05$ .
- Detection of a deviation from the RAR functional form Eq. (13) at  $> 5\sigma$  in galaxy rotation-curve data with intrinsic scatter beyond the SPARC error budget.
- Detection of a non-MOND-class transition acceleration  $g_{\dagger}$  that differs from  $1.13 \times 10^{-10} \text{ m/s}^2$  (Einstein frame) at  $> 5\%$ .

## VIII. INTERNAL CONSISTENCY AND CONVERGENCE

The dark-matter sector is internally consistent in three ways. First, the Avrami profile Eq. (8) and the MOND scale  $g_{\dagger}$  are derived independently from the Allen–Cahn equation and the Yukawa mass; they converge on the same observed RAR. Second, the two channels — conformal galactic and disformal cosmological — are separated by the same Avrami screening factor  $(1-P)^2$  that sets the susceptibility  $\chi_{\text{Avr}}$  in the disformal coupling. Third, the smoking-gun cluster ratio  $M_{\text{lens}}/M_{\text{dyn}}(z = 1.5) = 1.30$  uses the same  $P_0 = 0.851$  that enters the conformal channel, the disformal sector, and the cosmological background.

The convergence of these three independent inputs on the same set of empirical predictions is itself a non-trivial structural check.

## IX. DISCUSSION

### A. Summary of the framework

The Allen–Cahn condensation of the Brans–Dicke amplitude  $P$  on the 600-cell graph yields the Avrami profile  $P(g) = 1 - \exp(-\sqrt{g/g_{\dagger}})$  as the static gravitationally-driven solution. The conformal physical metric  $\tilde{g}_{\mu\nu} = P g_{\mu\nu}$  then produces the observed RAR with  $g_{\dagger} = 1.130 \times 10^{-10} \text{ m/s}^2$  matching Milgrom at 2.4%. SPARC fits with this prescription are comparable to MOND on

real data ( $\chi^2/\text{dof} \sim 2.4$ ), favourable on the synthetic-LIKE benchmark, and uniquely produce the smoking-gun  $M_{\text{lens}}/M_{\text{dyn}}$  turnover at  $z \sim 1.5$  peaking at 1.30.

### B. Relationship to existing frameworks

DCT reproduces MOND [5, 6] in the deep-MOND regime and differs at the few-percent level at intermediate accelerations. Unlike MOND, DCT provides a relativistic completion through the Brans–Dicke scalar–tensor action of the canonical framework [1] (matter minimally coupled to  $\tilde{g}_{\mu\nu} = P g_{\mu\nu}$ ; cf. Bekenstein TeVeS [17]). Unlike  $\Lambda\text{CDM}$ , DCT predicts  $\sigma_{\text{SI}} = 0$  exactly, in tension with WIMP detection scenarios but consistent with current nulls [10]. The smoking-gun  $M_{\text{lens}}/M_{\text{dyn}}$  turnover distinguishes DCT from both alternatives.

### C. Status of derived quantities

- $g_{\dagger}$  Einstein-frame:  $1.130 \times 10^{-10} \text{ m/s}^2$  (canonical paper-level; 2.4% match to Milgrom).
- $g_{\dagger}$  Jordan-frame:  $1.224 \times 10^{-10} \text{ m/s}^2$  (0.81 $\sigma$  match to Milgrom).
- SPARC fit: per-galaxy real-data  $\chi^2/\text{dof} \approx 2.4$  (comparable to MOND); synthetic 175-galaxy benchmark 1.141; stacked real-data boxed-line 0.97 (DCT\_E03 [1]).
- DM-to-baryon ratio:  $1/P_0 - 1 = 0.175$  from Wald entropy;  $\Lambda\text{CDM}$  measured  $\sim 0.18$ . Match.
- $M_{\text{lens}}/M_{\text{dyn}}(z = 1.5) = 1.30$  peak. Smoking-gun observable for Euclid 2027–2029.
- Splashback  $R_{\text{sp}}/R_{200} = \sqrt{P_0} = 0.923$ . DES Y3 [16] trends below  $\Lambda\text{CDM}$  (observed  $\sim 0.86$ ); DCT trends in the right direction but the precision is not yet decisive.

### D. Remaining open questions

- Splashback formula reconciliation: DCT corpus has parallel  $\sqrt{P_0} = 0.923$  (universal, cosmological) and  $1.02 \times P(R_{200})$  (local) formulae [1]. The observational predictions are close (0.923 vs. 0.949) but theoretically distinct; a single canonical choice is needed.
- Cluster-scale physics: at  $r_{500}$ , the conformal channel alone produces a 29% deficit relative to observed cluster mass. The disformal channel fills the gap, but a precise prediction at the level of cluster-mass-vs-temperature scaling has not been derived.

3. Avrami exponent first-principles derivation:  $n_A = 1/2$  is consistent with the Allen–Cahn similarity solution but a fully rigorous derivation from the diffusion-limited gravitational driving is still outstanding (DCT\_03 provides a sketch [1]).

### E. Computational implementation

A reproducible Python implementation of the DM-sector predictions, taking  $\omega_0$  and  $P_0$  as inputs and outputting  $g_{\dagger}$ , the RAR functional form, the cluster  $M_{\text{lens}}/M_{\text{dyn}}$  profile, and the splashback ratio, is available at the companion code repository [22]. The script also handles the Einstein-frame vs. Jordan-frame conversion explicitly and is parametric in the dataset choice (synthetic SPARC-LIKE vs. real LMS 2016).

## X. CONCLUSION

Dimensional Coherence Theory derives the radial-acceleration relation from the Allen–Cahn condensation

of the Brans–Dicke amplitude on the 600-cell graph, with the MOND scale  $g_{\dagger} = 1.130 \times 10^{-10}$  m/s<sup>2</sup> matching Milgrom’s measurement at 2.4% in the Einstein frame and  $0.81\sigma$  in the Jordan frame. SPARC fits are comparable to MOND on real data [4]; the synthetic 175-galaxy benchmark gives a more favourable result that we honestly distinguish from the real-data fit.

The smoking-gun observable distinguishing DCT from  $\Lambda$ CDM and MOND is the lens-to-dynamical mass ratio of galaxy clusters: a turnover at  $z \sim 1.5$  peaking at 1.30, falsifiable by Euclid 2027–2029. Direct dark-matter detection in DCT is exactly zero; current null results are consistent.

The dark-matter sector is therefore one of the strongest empirical legs of DCT — more accurately, the framework is most predictive at galaxy scales (where it derives the RAR from a single transition acceleration) and least predictive at homogeneous cosmological scales (where the legacy background-BAO  $\Delta\chi^2$  narrative is **retracted**: homogeneous  $P(t)$  cancels in radial null  $\chi(z)$ ; live interface is perturbation kernels and cluster tests [2]). The perturbation-level live programme on a  $\Lambda$ CDM background [2] retains the dark-matter-sector predictions presented here.

- 
- [1] N. G. Parrott, “Dimensional Coherence Theory: unifying quantum mechanics, general relativity, and the Standard Model,” Zenodo [10.5281/zenodo.18703512](https://zenodo.org/record/18703512) (2026).
  - [2] N. G. Parrott, “A background-BAO no-go theorem and the perturbation-level program in Dimensional Coherence Theory,” Zenodo [10.5281/zenodo.20032803](https://zenodo.org/record/20032803) (2026).
  - [3] S. S. McGaugh, F. Lelli, and J. M. Schombert, “Radial acceleration relation in rotationally supported galaxies,” *Phys. Rev. Lett.* **117**, 201101 (2016).
  - [4] F. Lelli, S. S. McGaugh, and J. M. Schombert, “SPARC: Mass models for 175 disk galaxies with Spitzer photometry and accurate rotation curves,” *Astron. J.* **152**, 157 (2016).
  - [5] M. Milgrom, “A modification of the Newtonian dynamics as a possible alternative to the hidden mass hypothesis,” *Astrophys. J.* **270**, 365 (1983).
  - [6] B. Famaey and S. S. McGaugh, “Modified Newtonian dynamics (MOND): observational phenomenology and relativistic extensions,” *Living Rev. Relativ.* **15**, 10 (2012).
  - [7] S. M. Allen and J. W. Cahn, “A microscopic theory for antiphase boundary motion and its application to antiphase domain coarsening,” *Acta Metall.* **27**, 1085 (1979).
  - [8] M. Avrami, “Kinetics of phase change. I. General theory,” *J. Chem. Phys.* **7**, 1103 (1939).
  - [9] M. Avrami, “Kinetics of phase change. II. Transformation-time relations for random distribution of nuclei,” *J. Chem. Phys.* **8**, 212 (1940).
  - [10] J. Aalbers *et al.* (LZ Collaboration), “First dark matter search results from the LUX-ZEPLIN (LZ) experiment,” *Phys. Rev. Lett.* **131**, 041002 (2023).
  - [11] E. Aprile *et al.* (XENON Collaboration), “First dark matter search with nuclear recoils from the XENONnT experiment,” *Phys. Rev. Lett.* **131**, 041003 (2023).
  - [12] Y. Meng *et al.* (PandaX Collaboration), “Dark matter search results from the PandaX-4T commissioning run,” *Phys. Rev. Lett.* **127**, 261802 (2021).
  - [13] J. Aalbers *et al.* (DARWIN Collaboration), “DARWIN: towards the ultimate dark matter detector,” *JCAP* **2016**, 017 (2016).
  - [14] B. P. Abbott *et al.* (LIGO Scientific and Virgo and Fermi GBM and INTEGRAL), “Gravitational waves and gamma-rays from a binary neutron star merger: GW170817 and GRB 170817A,” *Astrophys. J. Lett.* **848**, L13 (2017).
  - [15] Euclid Collaboration, R. Scaramella *et al.*, “Euclid preparation: cosmological constraints from the cosmic shear power spectra,” *Astron. Astrophys.* **684**, A82 (2024).
  - [16] T. M. C. Abbott *et al.* (DES Collaboration), “Dark Energy Survey Year 3 results: cosmological constraints from galaxy clustering and weak lensing,” *Phys. Rev. D* **105**, 023520 (2022).
  - [17] J. D. Bekenstein, “Relativistic gravitation theory for the modified Newtonian dynamics paradigm,” *Phys. Rev. D* **70**, 083509 (2004).
  - [18] P. Li, F. Lelli, S. McGaugh, and J. Schombert, “Fitting the radial acceleration relation to individual SPARC galaxies,” *Astron. Astrophys.* **615**, A3 (2018).
  - [19] R. M. Wald, *General Relativity* (University of Chicago Press, 1984).
  - [20] J. D. Bekenstein, “Relation between physical and gravitational geometry,” *Phys. Rev. D* **48**, 3641 (1993).
  - [21] T. S. Koivisto, D. F. Mota, and M. Zumalacárregui, “Screening modifications of gravity through disformally coupled fields,” *Phys. Rev. Lett.* **109**, 241102 (2012).

- [22] N. G. Parrott, “DCT-DM-01: dark-matter sector reproducibility code,” [GitHub repository](#) (2026), companion code to this paper.
- [23] G. W. Horndeski, “Second-order scalar–tensor field equations in a four-dimensional space,” *Int. J. Theor. Phys.* **10**, 363 (1974).
- [24] B. Bertotti, L. Iess, and P. Tortora, “A test of general relativity using radio links with the Cassini spacecraft,” *Nature* **425**, 374 (2003).
- [25] C. M. Will, “The confrontation between general relativity and experiment,” *Living Rev. Relativ.* **17**, 4 (2014).